SI Text

Internal Structural Difference of the γ-Subunit in the Ka and Me Structures. SI Fig. 5 shows the C^{α} atoms of the γ-subunit in the Ka structure (red) superimposed on the γ-subunit in the Me structure (blue). *a* shows the superposition of the entire γ-subunit (RMSD of 4.93 Å), where Ka: γ5-276 is overlapped with Me:γ1-272; the missing residues in the crystal (Me:γ58-66, 97-100, 118-126, and 151-156, and Ka:γ60-70) are excluded from the superposition. *b* shows the superposition of the γ-subunit taking into consideration potential amino acid insertions detected with sequence alignment using BLAST (given below: query is bMF_1-γ and subject is yMF_1-γ); i.e., Me:γ1-58, 59-99, 105-151, 151-194, and 195-272 are mapped to Ka:γ1-58, 65-105, 106-152, 155-198, and 200-277. The resulting superposition leads to a somewhat smaller RMSD of 3.53 Å. The only notable difference between the two structures in the coiled-coil (bMF_1 numbering γ:1-54, 209-272) part is that the C-terminal helix has a small kink in the Ka structure near the region of residue 250 (yMF_1 numbering), where the corresponding helical region in the Me γ structure is less curved (see black arrow in SI Fig. 5).

```
Query  1    ATLKDITRRLKSIKNIQKITKSMKMVAAAKYARAERELKPARVYGVGSLALYEKADIK--  58
            ATLK++  RLKSIKNI+KITK+MK+VA+ + ++AE+    A+          Y+ A+ K
Sbjct  1    ATLKEVEMRLKSIKNIEKITKTMKIVASTRLSKAEKAKISAKKMDEAEQLFYKNAETKNL  60

Query  59   ----TPEDKKKHLIIGVSSDRGLCGAIHSSVAKQMKSEAANLAAAGKEVKIIGVGDKIRS  114
                T     K LI+ ++SD+GLCG+IHS +AK ++    +   A     I+ +GDKI+
Sbjct  61   DVEATETGAPKELIVAITSDKGLCGSIHSQLAKAVRRHLNDQPNA----DIVTIGDKIKM  116

Query  115  ILHRTHSDQFLVTFKEVGRRPPTFGDASVIALELLN--SGYEFDEGSIIFNRFRSVISYK  172
             L RTH +   ++   +G+  PTF ++++IA +LL+      + + SI +N   S +S++
Sbjct  117  QLLRTHPNNIKLSINGIGKDAPTFQESALIADKLLSVMKAGTYPKISIFYNDPVSSLSFE  176

Query  173  TEEKPIFSLDTISSAESMSIYD-DIDADVLRNYQEYSLANIIYYSLKESTTSEQSARMTA  231
               EKPIF+  TI  + S   ++ D DA+V R+  EY+LAN +  ++ +   +E SAR  A
Sbjct  177  PSEKPIFNAKTIEQSPSFGKFEIDTDANVPRDLFEYTLANQMLTAMAQGYAAEISARRNA  236

Query  232  MDNASKNASEMIDKLTLTFNRTRQAVITKELIEIISGAAAL  272
             MDNASKNA +MI++ ++ +NRTRQAVIT EL++II+GA++L
Sbjct  237  MDNASKNAGDMINRYSILYNRTRQAVITNELVDIITGASSL  277
```

Definition of the Rotation Angle. The reference vector used for the γ-orientation is calculated from the crystal coordinates of Ka, as the projection of the averaged vector that connects residue 84 with residue *i* (*i* = 85-100) onto the plane defined by residues 19 in the three β-subunits. The γ-angle for a simulated structure is then computed as the angle between the instantaneous

projection defined in the same way and the reference vector. The definition used here is similar to that used by Koga and Takada (KT) (1); the difference is due primarily to our use of the yMF_1 structure Ka, rather than the bMF_1 structure Ab.

Control Simulations Using Ab as the Starting Crown Structure. SI Fig. 7 shows the γ-angle in a simulation where the crown structure of Abrahams *et al.* (2) reported in 1994 (Ab) [Protein Data Bank (PDB) entry 1BMF] is used for ATP binding. To obtain an Ab crown structure compatible with the Ka γ-subunit, the simulation starts from the Ka structure (crown plus γ) using the protocol described in the text. The crown structure is then gradually changed (with TMD and PNM) to that in Ab while the γ-stalk is described by an elastic network corresponding to Ka. This transition results a γ-rotation of -10° (i.e., toward the synthesis direction), compared with the Ka structure. The ATP binding is then simulated by changing the crown structure from Ab to Me (i.e., β_E to β_{TP}, β_{DP} to β_{HC}, and β_{TP} to β_{DP}), which yields a γ-rotation of approximately 95° in the hydrolysis direction. The final transition of the crown from Me back to Ab introduces a further 25° γ-rotation. Results are only shown for a representative trajectory; independent simulations display essentially the same feature. The major difference between the Ab and Ka crown structures is that the α_{DP}/β_{DP} interface in the Ab structure adopts a tight closed conformation as a consequence of binding ADP/Mg^{2+}, very likely in an azide inhibited state (3). This interface is slightly more open (the β_{HO} conformation) with an ATP analog (AMP-PNP) bound in the Ka structure. Starting ATP binding with the Ab crown, in which the hydrolysis products are bound with a closed β_{DP} conformation (rather than the "half-open" β_{HO} found in Ka), a greater substep rotation for ATP binding (95°) and a smaller substep for product release (25°) are obtained, compared with the 85°/35° substep rotations obtained if the Ka crown is used. The relatively small difference between the Ka → Me → Ka and Ab → Me → Ab results supports the robustness of the simulations and the importance of using actual crystal structures for the conformational states.

A Typical Torque Profile During the 85° Rotation. SI Fig. 8 shows a typical calculated torque profile (in units of pN nm) as a function of time during an 85° substep rotation. The time period 0-220 ps corresponds to the time period 200-420 ps in SI Fig. 9. The instantaneous torque

generated during the 85° substep rotation varies with time and the rotation angle. Thus, we used an average value for the absolute torque to make a comparison with the experimentally measured torque (see below, *Absolute Torque Magnitude in the Simulations*). It has been suggested (4) that a uniform torque generation is required for the motor to achieve its high efficiency. Using long actin filaments (~μM) as the frictional load, which makes the turnover of the motor much slower than the load-free F_1, Yasuda *et al.* (5) observed an almost constant torque generation. The use of long filaments as the frictional torque reporter has been criticized, since the rotation is significantly slowed down, and the rotation signals involve relaxation of the filament and may not reflect the actual torque generation. Junge and coworkers (6) addressed this issue by developing a protocol to extract the torque magnitude from the curvature (rather than the angular velocity) of the filament. They found a nonuniform distribution of torque generated along the angular reaction coordinate. Detailed examination of the torque profile along the rotation is also limited by the temporal resolution of many of the single-molecule experiments. Higher time resolution experiments that directly monitor the rapid γ-rotation (7) should be useful for addressing the details of the torque generation. The torque on the γ-subunit we observed during the rapid ATP driven rotation is not directly comparable with any of the experiments because of the differences in the rotational time scale and load. The nonconstant torque generation observed in the simulation may reflect the varying β/γ coupling strength for the dynamical configurations sampled during the rapid γ-rotation and the stochastic nature of the simulation. Given that frictional solvent damping was not present, we have not attempted to obtain statistically meaningful results by averaging over a series of trajectories.

Absolute Torque Magnitude in the Simulations. To obtain the rotation of the γ-subunit on the simulation time scale (subnanosecond rather than submillisecond), a torque based on the β/γ repulsion (Eq. **2**) is expected to be greater than the physical one generated in the actual F_1-ATPase rotation. Because the torque varies along the γ-rotation (see SI Fig. 8), we compare the torque value averaged over the substep rotation. The average values of the torque generated during the 85° and 35° substeps are 784 and 184 pN nm (approximately in the ratio of 4/1), respectively. This value is 4-16 times greater than that of the average torque of 40-50 pN nm estimated from experiment (7, 8). That a significantly greater torque was not required is due, at

least in part, to the fact that there is no solvent damping, whereas the physical system is overdamped. In a molecular dynamics simulation with an all-atom description of F_1-ATPase including explicit solvent (9), a torque, which is approximately 50 times greater than the experimental values, was able to rotate the γ-subunit by 120° in the synthesis direction in 1 ns.

Distances of β_E:L391-γ:M25 and β_E:L391-γ:K237 During the 85° Rotation. SI Fig. 9 plots the time series of the distance between β_E:L391-γ:M25 (blue curve) and that of the β_E:L391-γ:K237 (red curve) for a representative trajectory of the 85° rotation simulation. The data for the first 200 ps and last 180 ps shown on SI Fig. 9 correspond to equilibration, and the middle 220 ps account for the transition from the Ka crown to the Me crown (the black arrow is used to mark the start of the crown transition). During the crown conformational change, the distance of β_E:L391-γ:M25 is greatly reduced from its preequilibrium value (22 Å) to a minimum (5 Å), where a strong repulsive interaction between β and γ occurs due to the formation of a tightly coupled β/γ interface that generates a torque and converts β motion into γ-rotation. The other distance (β_E:L391-γ:K237) also decreases during the reduction of β_E:L391-γ:M25 distance, although the reduction of the former somewhat lags behind that of the latter. At the minimum of the β_E:L391-γ:M25 curve (at t = ~280ps on SI Fig. 9, which corresponds approximately to a 40° rotation from the ATP waiting γ position), the β_E:L391-γ:K237 distance is still greater than 8 Å. This indicates that the reduction of the β_E:L391-γ:K237 distance is a consequence of the rotation of γ, rather than the driving force of such rotation during this part of the cycle. As the γ-rotation progresses, the β_E:L391-γ:M25 distance increases after its minimum, indicative of the weakening of the β/γ coupling through this interaction. The distance of β_E:L391-γ:K237 continues to decrease until a minimum of less than 5 Å is reached at t = ~350 ps. This corresponds to the shift of the β/γ coupling interface from N-terminal helix bulge (γ:M25) to the C-terminal helix bulge (γ:K237), in accord with results of the torque analysis (see Fig. 3 and discussion in the text).

Sequence Alignment of the β/γ Coupling Interface in the F_1-ATPase Family. The torque analysis identified four clusters (γ:20-25, 75-79, 232-238, 252-258, bMF_1 numbering) of the γ-subunit that make the primary contribution to the rotational torque. Sequence alignments of the β- and γ-subunits in F_1-ATPase, for bovine mitochondrial F_1 (bMF_1), yeast mitochondrial F_1

(yMF_1), thermophilic bacteria *Bacillus* PS3 F_1 (TF_1.*Bacillus* PS3), *Escherichia coli*. F_1 (EcF_1), and chloroplast F_1 (cF_1). In the cluster γ20-25 identified from the torque analysis, hydrophobic residues γ:M23, M25 and V26 are strictly conserved. These hydrophobic residues on the N-terminal helix of the γ coiled-coil are likely to form an efficient β/γ coupling interface with β_E:I390 and L391, which are also highly conserved for the species we examined. Another conserved residue identified is γ:L77, which is involved in the 35° rotation.

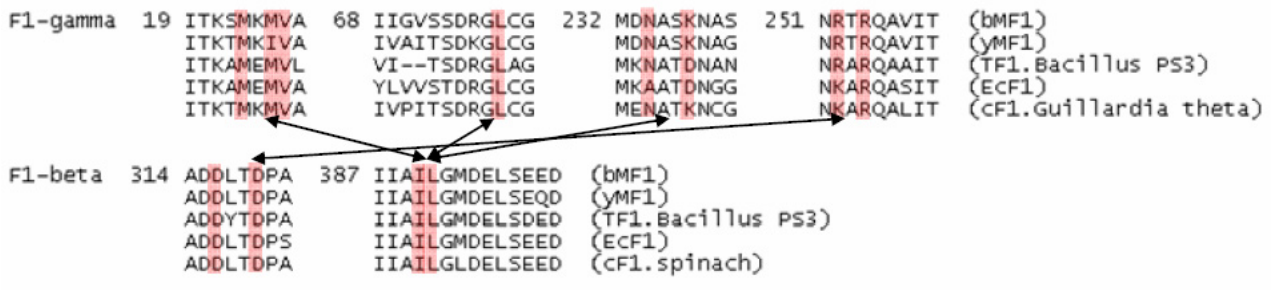

Comparison with KT "Tri-Site" Simulation. KT (1) also studied what they called a "tri-site" model with their method and reported that their simulations did not show substeps and did not always show the correct rotation direction. The model used by KT starts with the Ab structure and generates an artificial noncrystallographic structure to represent the state after ATP binding; all of the subunit conformations are taken from the Ab structure, which is β_E, β_{DP}, β_{TP} in our notation, and is suddenly switched to β_{TP}, β_{DP}, β_{TP}. KT suggest the problem is with the use of the Ab structure, but as we point out (see above, *Control Simulations Using Ab as the Starting Crown Structure*), its use yields results similar to those obtained with the Ka structure. Apparently, the problem arises from the use of the artificial, fully closed structure (i.e., all subunits are in the closed conformation) that KT created; there is no reason to believe that it can exist. By contrast, we used the known Me structure as the intermediate state with ligands in all three subunits.

Details of the Plastic Network Model (PNM) Used in the Simulations. The energy contribution $E_i^{\mathrm{A}}(\vec{x})$ of the *i*th stable state (i = 1,2) of network A and the energy of the plastic network A connecting these stable states (E^{A}) are given by [note these energies are described as effective elastic free energies (G) in the original reference (10)]:

$$E_i^{\mathrm{A}}(\vec{x}) = \sum_{a,b\in \mathrm{A}}^{N_{\mathrm{A}}} \frac{k_i^{\mathrm{A}}}{2}(r_{ab} - r_{ab}^{[i]})^2 \quad \textbf{[4]}$$

$$E^{\mathrm{A}} = \frac{E_1^{\mathrm{A}} + E_2^{\mathrm{A}} - \sqrt{(E_1^{\mathrm{A}} - E_2^{\mathrm{A}})^2 + 4(\varepsilon^{\mathrm{A}})^2}}{2} \quad \textbf{[5]}$$

where A defines the state represented by the network, N_{A} denotes the number of atoms in network A, and ε^{A} denotes the coupling term between the two end states; k_i^A is the elastic constant for ith stable basin of the PNM labeled A; r_{ab} and $r_{ab}^{[i]}$ denote the distance between atom a and b for an instantaneous dynamical structure and that in the reference i (i = 1 or 2) network structure, respectively. For the central γ-stalk, a simple elastic network is used on the assumption that it does not change its conformation significantly during the ATP hydrolysis cycle. The following parameters were used as the elastic constant and the coupling constant (ε) for the networks: $k^{\alpha 3\beta 3}$ = 2.67 kcal/mol/Å^2, k^{γ} = 1.88 kcal/mol/Å^2, and $\varepsilon^{\gamma} = \varepsilon^{\alpha 3\beta 3}$ = 1.0 kcal/mol. The networks were generated with a distance cutoff of 14 Å to balance protein flexibility and simulation stability. The coarse-grained model parameters must be such that the system is sufficiently rigid that the conformational changes on a ps/ns time scale mimic those expected on the physical time scale. The use of different strengths for the elastic constants of the PNMs changes the quantitative result slightly, but the qualitative behavior of the 85°/35° substep rotations remains the same. SI Fig. 10 shows the γ-angles of 10 simulations using a different set of elastic constants for the PNM: $k^{\alpha 3\beta 3}$ = 5.0 kcal/mol/Å^2 and k^{γ} = 5.0 kcal/mol/Å^2, where all other parameters and the simulation protocols remain unchanged, as described in the text. With these parameters, the result is a 93°/27° substep rotation.

Missing Residues Modeling. The initial state of the model (Ka) is constructed based on a crystal structure of the yeast mitochondrial F_1-ATPase (PDB entry 2HLD) solved by Kabaleeswaran. *et al.* (11). Initial coordinates for missing residues (α_E:408-409; α_{TP}:408-409; γ:60-70) were obtained with a loop building utility in Swiss-PdbViewer (12). These patched residues were relaxed using molecular dynamics with the CHARMM22 force field (13) in the presence of

GBSW implicit solvation (14) with all nonmissing residues fixed and annealed to 50 K. The C^{α} atom coordinates in the final structure were used to build the coarse-grained model for these missing residues. For the Me structure (PDB entry 1H8E) (15), the positions of C^{α} atoms for missing residues (α_E:404-409; α_{TP}:402-409; α_{DP}: 405-408; β_E:127-128, 465-474; and γ:58-66, 97-100, 118-126, 151-156) in the crystal structure were obtained from a TMD simulation that carries the available backbone coordinates from an all-atom intact F_1 model to those defined in the Me structure, where the same potential was used. The intact F_1 all-atom model was obtained following a previous procedure (16) that combines the nucleotide-bound Ab crown structure with the DCCD inhibit structure for the same enzyme where the entire central stalk was available (17). To establish the correct mapping for the TMD simulations among the Me, Ka, and Ab structures, the coarse-grained model only retains residues 26-509 for the α-subunits, 9-474 for the β-subunits, and 1-276 for the γ-subunits (yMF_1 numbering). Note that for the Ka structure, residues 26-509 (yMF_1 numbering) of the α-subunits are mapped to residues 24-507 (bMF_1 numbering) in the model to retain structural consistency.

Additional Details on the Restraints Used in the Simulations. In the present simulations, we applied a harmonic restraint to the center of mass (COM) of the γ-subunit to prevent the central stalk from tilting during the TMD guided conformational transition. This type of COM restraint was used previously in an external torque induced simulation at the ATP synthesis direction to obtain stable dynamics (9). A uniform spring constant of 5.0 kcal/mol/Å^2 was used for the COM restraints. KT used different restraints in simulating the F_1 rotation based on their funnel models; they tethered the C-terminal tip of the γ-subunit with a spring force, as well as the β-subunit heads (1), although the immobilization of the γ-tip is not explicitly present in the single-molecule experiment. Without such restraints, the γ-stalk "flys" out from the central cavity formed by $\alpha_3\beta_3$ during fast conformation switching, due to large repulsive interaction that couples the γ-subunit with surrounding protein subunits.

MD Simulation Details. With the elastic networks defined from the structure Ka, the system is first equilibrated at 50 K with the restraints described above (see above, *Additional Details on the Restraints Used in the Simulations*) for a period of 1 ns. Following the equilibration, TMD

simulations of the $\alpha_3\beta_3$-crown were initiated and the conformation was transformed to the Me $\alpha_3\beta_3$-crown during a period of 220 ps (Δrmsd = 0.0002 Å/MD step), with the γ conformation from Ka. After 600 ps further equilibration with the Me crown, the $\alpha_3\beta_3$ subcomplex is gradually (over 130 ps) transformed back to the Ka structure corresponding to the conformation after one ATP hydrolysis cycle. The system was finally equilibrated for another 1 ns until a plateau region of the γ-rotational angle was reached.

Description of Mutation Studies. Many mutant studies and conservation analyses (see above, *Sequence Alignment of the β/γ Coupling Interface in the F_1-ATPase Family*) have been made to provide information concerning the residues that play role in the rotational mechanism. The importance of residues in the γ20-25 region (for example, a highly conserved residue γM23 in the F_1-ATPase family; see above, *Sequence Alignment of the β/γ Coupling Interface in the F_1-ATPase Family*), has been demonstrated by many investigators using various mutants (18-22). In particular, mutating M23 to a charged residue Lys in TF_1 has been shown to reduce the hydrolysis activity to 2.3%, while the corresponding Cys mutant retains more of the activity, suggesting a disruption of the hydrophobic interaction of the M23K mutant (20). The importance of residues in this region (e.g., γ:M25) has also been noted in other simulations (1, 9). Alanine mutation studies by Hara and coworkers (23) suggested that side chains of the conserved DELSEED motif of the β-subunit (TF_1:390-396) and the corresponding close-contacting γ-subunit region (TF_1:L85,R95) do not play a direct role in torque generation.

Possible Additional Substeps. One question raised by an anonymous referee is whether the small peak at approximately 20° in Fig. 2 is significant and indicates an additional rotational substep. Besides the major substeps separated by relatively long dwell periods (on a millisecond time scale), there could be additional (but much shorter) intermediate rotational substeps that are not captured by experimental measurements with limited temporal resolution. A technique that may be sensitive enough to directly monitor the signal of rapid γ-rotation was reported in a recent paper by Spetzler *et al.* (7). In addition to the major characteristics of the γ-rotation, such as the average angular velocity and frictional torques, the authors also presented a swath of γ-angular profiles during the rapid γ-rotation (see their figure 6B); the behavior of the trajectories

shows a great deal of diversity: a distribution of slopes in the angular increase and various short pauses exist. The 20° substep pause found in our simulation may belong to this category. However, given the approximations in the model and limited statistics, we feel that the apparent substep at 20° is too small to be significant.

1. Koga N, Takada S (2006) *Proc Natl Acad Sci USA* 103:5367-5372.
2. Abrahams JP, Leslie AGW, Lutter R, Walker JE (1994) *Nature* 370:621-628.
3. Bowler MW, Montgomery MG, Leslie AGW, Walker JE (2006) *Proc Natl Acad Sci USA* 103:8646-8649.
4. Oster G, Wang H (2000) *J Bioenerg Biomembr* 32:459-469.
5. Yasuda R, Noji H, Kinosita K, Jr, Yoshida M (1998) *Cell* 93:1117-1124.
6. Pänke O, Cherepanov DA, Gumbiowski K, Engelbrecht S, Junge W (2001) *Biophys J* 81:1220-1233.
7. Spetzler D, York J, Daniel D, Fromme R, Lowry D, Frasch W (2006) *Biochemistry* 45:3117-3124.
8. Kinosita K, Jr, Adachi K, Itoh H (2004) *Annu Rev Biophys Biomol Struct* 33:245-268.
9. Böckmann RA, Grubmüller H (2002) *Nat Struct Biol* 9:198-202.
10. Maragakis P, Karplus M (2005) *J Mol Biol* 352:807-822.
11. Kabaleeswaran V, Puri N, Walker JE, Leslie AGW, Mueller DM (2006) *EBMO J* 25:5433-5442.
12. Guex N, Peitsch MC (1997) *Electrophoresis* 18:2714-2723.
13. MacKerell AD, Jr, Bashford D, Bellott M, Dunbrack RL, Jr, Evanseck JD, Field MJ, Fischer S, Gao J, Guo H, Ha S, *et al.* (1998) *J Phys Chem B* 102:3586-3616.
14. Im W, Lee MS, Brooks CL, III (2003) *J Comput Chem* 24:1691-1702.
15. Menz RI, Walker JE, Leslie AGW (2001) *Cell* 106:331-341.
16. Ma J, Flynn TC, Cui Q, Leslie AGW, Walker JE, Karplus M (2002) *Structure* 10:921-931.
17. Gibbons C, Montgomery MG, Leslie AGW, Walker JE (2000) *Nat Struct Biol* 7:1055-1061.
18. Shin K, Nakamoto RK, Maeda M, Futai M (1992) *J Biol Chem* 267:20835-20839.
19. Nakamoto RK, Maeda M, Futai M (1993) *J Biol Chem* 268:867-872.
20. Bandyopadhyay S, Allison WS (2004) *Biochemistry* 43:9495-9501.

21. Omote H, Sambonmatsu N, Saito K, Sambongi Y, Iwamoto-Kihara A, Yanagida T, Wada Y, Futai M (1999) *Proc Natl Acad Sci USA* 96:7780-7784.
22. Al-Shawi MK, Nakamoto RK (1997) *Biochemistry* 36:12954-12960.
23. Hara KY, Noji H, Bald D, Yasuda R, Kinosita K, Jr, Yoshida M (2000) *J Biol Chem* 275:14260-14263.